Testing convective parameterizations with tropical measurements of HNO_3, CO, H_2O, and O_3: Implications for the water vapor budget

Ian Folkins,[1] P. Bernath,[2] C. Boone,[2] L. J. Donner,[3] A. Eldering,[4] Glen Lesins,[1] R. V. Martin,[1,6] B.-M. Sinnhuber,[5] and K. Walker[2]

Received 21 March 2006; revised 7 July 2006; accepted 10 August 2006; published 14 December 2006.

[1] The updraft and downdraft mass flux profiles generated by convective parameterizations differ significantly from each other. Most convective parameterizations are tested against temperature and relative humidity profiles from radiosondes. Chemical tracers provide important additional constraints on the vertical redistribution of mass by convective parameterizations. We compile tropical climatologies of water vapor (H_2O), ozone (O_3), carbon monoxide (CO), and nitric acid (HNO_3) from a variety of satellite, aircraft, and balloon-based measurement platforms. These climatologies are compared with the profiles predicted by a variant of the Emanuel convective parameterization, a two-column model of the tropical atmosphere, and by the implementations of the Relaxed Arakawa Schubert (RAS) and Zhang and McFarlane (ZM) parameterizations in a three-dimensional global forecast model. In general, the models with more pronounced convective outflow in the upper troposphere compare more favorably with observations. These models are associated with increased evaporative moistening in the middle and lower troposphere.

Citation: Folkins, I., P. Bernath, C. Boone, L. J. Donner, A. Eldering, G. Lesins, R. V. Martin, B.-M. Sinnhuber, and K. Walker (2006), Testing convective parameterizations with tropical measurements of HNO_3, CO, H_2O, and O_3: Implications for the water vapor budget, *J. Geophys. Res.*, *111*, D23304, doi:10.1029/2006JD007325.

1. Introduction

[2] Increasing the concentration of carbon dioxide in the atmosphere reduces the emission of longwave radiation from the troposphere. In the absence of a change in the absorption of solar radiation in the troposphere, long-term energy balance implies that there must be an increase in tropospheric temperatures. The magnitude of this temperature increase is sensitive to the way in which tropospheric temperature changes interact with the hydrological cycle. In most models, a warming of the troposphere is associated with an increase in water vapor concentrations which approximately doubles the warming that would be obtained for fixed water vapor [*Stocker et al.*, 2001]. In some models, however, the water vapor feedback more than triples the surface temperature response [*Hall and Manabe*, 1999].

[3] The magnitude of the tropical water vapor feedback in a global climate model is mostly determined by how the model treats convection. In global models, convection is an unresolved process which must be parameterized. Convective clouds moisten the atmosphere by detraining saturated air into their environment, and by producing liquid water and ice, which evaporate as they fall through unsaturated air beneath precipitating clouds. On the larger scale, the net upward mass transport within convective clouds gives rise, by mass conservation, to an induced downward mass flux in the background atmosphere. Because water vapor mixing ratios typically decrease with altitude, this induced subsidence decreases the relative humidity of the background atmosphere. The convective parameterization of a climate model determines both the vertical variation of cloudy outflow of the model, as well as the amount of evaporative moistening associated with falling precipitation. Future changes in water vapor will be determined not only by changes in atmospheric temperatures, but also by changes in how convective clouds vertically redistribute mass and water vapor in the atmosphere. To accurately simulate the water vapor feedback, a model must reproduce the way in which clouds currently transport air and moisture vertically, as well as how this transport may evolve in the future.

[4] It is desirable to test the vertical transport of a convective scheme against a variety of chemical tracers. Cloud mass flux profiles generated by convective schemes are usually tested by comparison with temperature and

[1]Department of Physics and Atmospheric Science, Dalhousie University, Halifax, Nova Scotia, Canada.
[2]Department of Chemistry, University of Waterloo, Waterloo, Ontario, Canada.
[3]Geophysical Fluid Dynamics Laboratory, NOAA, Princeton University, Princeton, New Jersey, USA.
[4]Jet Propulsion Laboratory, Pasadena, California, USA.
[5]Institute of Environmental Physics, University of Bremen, Bremen, Germany.
[6]Also at Harvard-Smithsonian Center for Astrophysics, Cambridge, Massachusetts, USA.

0148-0227/06/2006JD007325

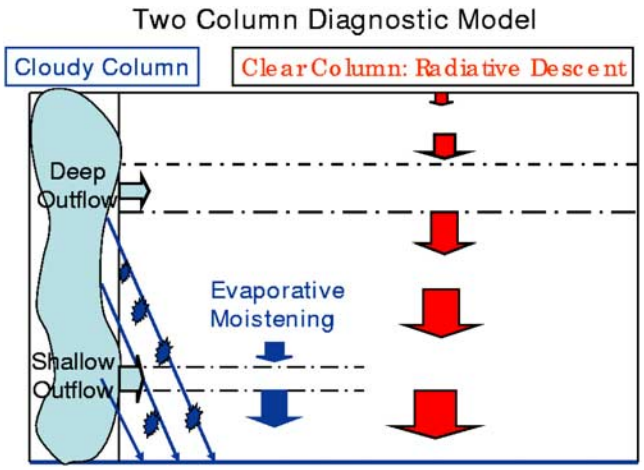

Figure 1. A simplified representation of the tropical atmosphere showing the assumptions of the two-column model (TCM) [*Folkins and Martin*, 2005]. Radiative descent in the clear sky column (red arrows) is calculated from tropical mean climatologies of trace gases and temperature. The vertical variation of evaporatively forced descent is constrained to agree with observed relative humidities. The vertical variation of outflow from the cloudy column is then determined by mass continuity, i.e., the assumption that the tropical atmosphere can be considered, to first order, a closed circulation.

water vapor measurements. The diversity of updraft and downdraft mass flux profiles generated by convective schemes suggests that these observational constraints are, by themselves, insufficient. In particular, most previous relative humidity vertical profiles comparisons have been confined to radiosondes, whose accuracy below −30 C is often poor [*Miloshevich et al.*, 2004]. For example, radiosondes fail to detect, or tend to underpredict, the rapid increase in relative humidity that occurs within the deep outflow layer, a layer of enhanced convective outflow starting near 10 km and extending to 17 km. The vertical variation of cloudy outflow in this layer is therefore poorly constrained in most convective parameterizations.

2. Model Description

[5] In this paper, tropical climatologies of water vapor (H_2O), ozone (O_3), carbon monoxide (CO), and nitric acid (HNO_3) are generated from a variety of measurement platforms. These climatologies are used to test the representation of convective transport in four models. Two of the models use assimilated meteorological data sets. The other two models are used in a one-dimensional framework. The two assimilated meteorological data sets were produced by the Goddard Earth Observing System (GEOS) at the NASA Global Modeling and Assimilation Office (GMAO). The GEOS-3 model uses the Relaxed Arakawa Schubert (RAS) convective parameterization [*Moorthi and Suarez*, 1992], while the GEOS-4 model uses the Zhang and McFarlane (ZM) convective parameterization [*Zhang and McFarlane*, 1995].

[6] The third model is based on a convective parameterization [*Emanuel*, 1991; *Emanuel and Zivkovic-Rothman*, 1999] that has been implemented in some global models [e.g., *Peng et al.*, 2004]. The version used here is coupled to an interactive radiative transfer model with more complete cloud physics and uses a fractional cloud scheme. It will be referred to as the CONRAD (Emanuel) model [*Bony and Emanuel*, 2001]. It is run with a fixed sea surface temperature of 27.5°C, and vertical resolution of 25 hPa. It is coupled to the Brewer-Dobson stratospheric circulation via an imposed upward vertical velocity. This vertical velocity linearly increases from zero at 250 hPa to 2.5×10^{-4} m/s at 150 hPa, and is constant above this pressure.

[7] The fourth model is a two-column model (TCM) [*Folkins and Martin*, 2005]. Its approach is illustrated in Figure 1. Radiative mass fluxes in the clear sky column were calculated from temperature, water vapor, and ozone measurements at twenty four high vertical resolution radiosonde and ozonesonde stations between 20°S and 20°N. These fluxes were then averaged together to produce a tropical mean clear sky radiative mass flux. In the upper troposphere, the downward radiative mass flux increases toward the surface. In the model, this increase is supplied by an outflow of air from the cloudy column. If it is assumed that this cloudy outflow is saturated, the model can be used to construct a primitive model of the tropical troposphere, containing no free parameters, which correctly predicts the observed increase in relative humidity between 11 km and 14 km [*Folkins et al.*, 2002b]. To obtain agreement with relative humidities in the middle and lower troposphere, an evaporative moistening source of water vapor is added to the clear sky column. The magnitude of this moisture source is tuned to give rise to the correct tropical mean relative humidity profile. The cooling associated with this evaporation drives an additional downward mass flux in the clear sky column which requires, by mass conservation, a shallow convective outflow from the cloudy column. This model can be considered to be the simplest possible representation of the tropical troposphere that is consistent with both observed temperatures and water vapor mixing ratios. Its most important deficiencies are probably (1) that it ignores the possibility of entrainment of air from the clear sky column into the cloudy column and (2) that it does not allow downdrafts to directly inject evaporatively chilled air into the boundary layer. Relaxation of either of these restriction would require closure assumptions which are still quite speculative. The one-dimensional approach of the TCM model is also probably more appropriate in the upper troposphere, where stronger horizontal winds decrease the magnitude of regional anomalies in chemical species.

[8] A cloudy updraft can moisten the surrounding atmosphere in the absence of a local net divergence. For example, an updraft can simultaneously entrain subsaturated air from its environment while detraining saturated air into its environment. If the rates of entrainment and detrainment are equal to each other, this combination of entrainment and detrainment would have no effect on the mass divergence of the cloud updraft at that altitude. It would, however, cool the updraft at that altitude, affecting its buoyancy and detrainment rate at other altitudes.

[9] The radiative heating rates of the clear sky column in the TCM model were calculated without taking clouds into account. Clouds can reduce the absorption of longwave

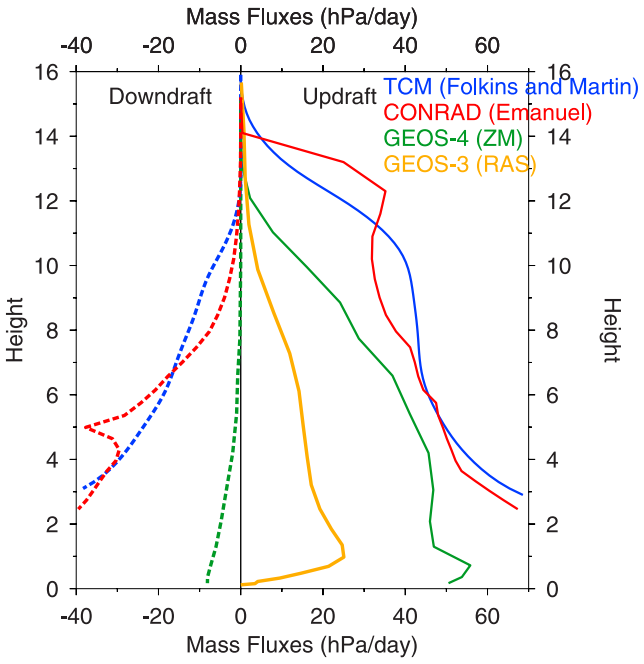

Figure 2. Updraft and downdraft mass fluxes of the four models. The GEOS-3 and GEOS-4 mass fluxes are a 20°S–20°N average over the four model output times on 1 July 2001. Other days are similar. The GEOS-3 model does not have a downdraft parameterization.

radiation in clear sky regions by reducing upwelling longwave radiation from the surface. For the most part, however, it is likely that the radiative effects of clouds are concentrated within clouds. The cloud mass flux diagnosed using the two-column approach represents the response to the sum of all sources of diabatic heating within clouds, including radiative heating.

[10] The TCM model treats the tropics (20°S–20°N) as a closed box. It has been shown, using GEOS assimilated winds, temperatures, and humidities, that the net exchange of mass, water vapor, and dry static energy between the tropics and extratropics does not significantly affect the tropical means budgets of these quantities at most altitudes [*Folkins and Martin*, 2005]. In the vicinity of the tropical tropopause, where the convective outflow is very weak, the exchange of mass between the tropics and extratropics is comparable to the detrainment rate. At these altitudes, the application of an adjustment to the detrainment rate to take this mass transport into account has some affect on the O_3 and CO mixing ratios predicted by the TCM model [*Folkins et al.*, 2006].

[11] It is useful to keep in mind that convection is ultimately a small-scale turbulent process, and that deep convective systems possess a complex three-dimensional structure. It is not clear that the representation of convective transport in terms of some combination of updrafts and downdrafts can in principle represent this process adequately [*Donner et al.*, 2001; *Yano et al.*, 2004].

3. Updraft and Downdraft Mass Fluxes

[12] The tropical mean (20°S–20°N) updraft and downdraft mass fluxes of the four models are shown in Figure 2. There are clearly significant differences between the models. The RAS convective parameterization in GEOS-3 does not have a representation of evaporative downdrafts. The downdraft mass flux of the GEOS-4 model is quite small at all altitudes. The downdraft mass fluxes of the TCM and CONRAD (Emanuel) models are small in the upper troposphere, so that above 10 km the cloud updraft mass flux in these two models is almost entirely balanced by radiative subsidence. The downdraft mass flux of these two models increases rapidly toward the surface, and eventually becomes larger than radiative subsidence.

[13] Some of the differences between the mass fluxes shown in Figure 2 arise from the way that convective schemes are implemented in global forecast models. The input of wind and temperature observations can give rise to spurious diabatic forcings in forecast models, especially if there is a bias in the way that the convective scheme represents convection. Perhaps more importantly, global forecast models generate two types of rainfall. In addition to the "convective" rainfall generated by the convective scheme, models also generate "stratiform" rainfall when the relative humidity at a particular grid point exceeds some threshold. The convective rainfall in forecast models is tuned so that the total convective plus stratiform rainfall is close to the observed tropical mean. Models with a larger stratiform component would therefore be expected to have weaker convective mass fluxes. Much of the condensational heating and associated vertical mass transport in these models would be associated with the stratiform rainfall component.

4. Entrainment and Detrainment Profiles

[14] The concentration of a chemical species in the background atmosphere can be affected by detrainment of updraft and downdraft air into the background atmosphere, and by entrainment of background air into updrafts and downdrafts. The net effect of convection on the concentration of a chemical species is determined by the sum of these four processes. Figure 3 shows the net cloud (updraft plus downdraft) entrainment and detrainment rates of the various models using dashed and solid lines. The entrainment and detrainment rates of the GEOS-3 model refer to updrafts only, as this model does not have a representation of downdrafts. In the case of the TCM model, only the detrainment rate is shown because this model does not allow for entrainment.

[15] The detrainment profiles of the GEOS-4, TCM, and CONRAD (Emanuel) models all exhibit an upper tropospheric maximum. There are, however, significant variations in the height and intensity of this maxima between the models. The detrainment profile of the GEOS-3 model does not exhibit a clearly defined deep outflow layer.

[16] It is likely that some of the differences in cloud outflow between the models shown in Figure 3 arise from differences in their treatment of updraft entrainment. The entrainment of subsaturated background air into convective updrafts leads to evaporation of cloud condensate. This evaporation decreases temperatures and buoyancies within updrafts, and reduces the average height of convective outflow. For example, the sharpness of the detrainment feature in the CONRAD (Emanuel) model appears to arise from the assumption that moist static energy is roughly

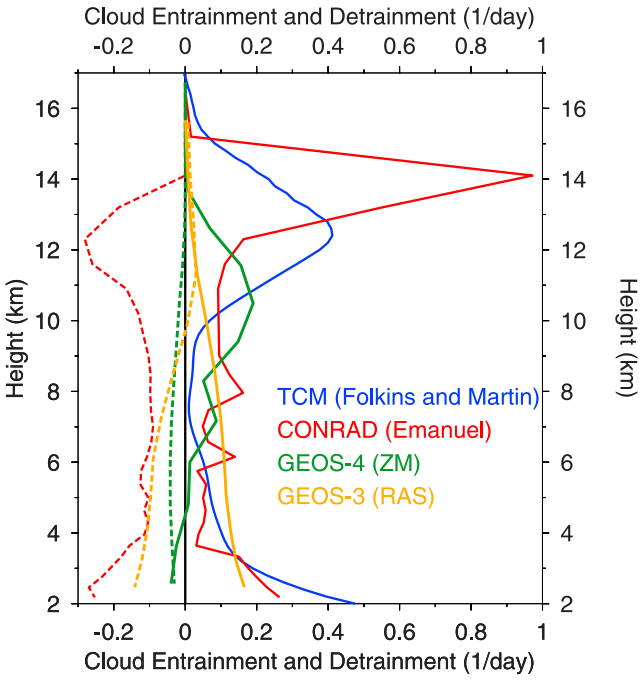

Figure 3. Entrainment (dashed) and detrainment (solid) rates of the GEOS-3, GEOS-4, and CONRAD (Emanuel) models. The TCM model does not have a provision for entrainment.

constant in the subcloud layer (below 950 hPa), and the use of a stochastic mixing parameterization that results in a significant fraction of the air within deep convective updrafts being transported to the upper troposphere in an almost undilute manner. The detrainment peak near 14 km therefore roughly corresponds to the level of neutral buoyancy of boundary layer air. The sharpness of this feature would likely be diminished when this model is coupled to a three-dimensional model with variable sea surface temperatures, and possibly, a different representation of boundary layer processes. It should be noted, however, that an interval of enhanced upper tropospheric divergence which peaks near 200 hPa (~12.5 km) is a common feature of most diagnostic studies of tropical convection [*Betts*, 1973; *Yanai et al.*, 1973].

5. Net Cloud Mass Fluxes

[17] In the tropical troposphere, the clear sky radiative heating rate is mainly determined by the vertical profiles of temperature and relative humidity. Convective parameterizations should have similar rates of clear sky radiative descent, to the extent that they drive the atmospheric temperature profile to a common moist adiabat, and are tuned to replicate relative humidity observations. Because radiative subsidence is approximately balanced by the net cloud (updraft plus downdraft) mass flux, one would expect the net cloud mass fluxes of convective parameterizations to be similar to each other.

[18] There are a number of reasons why the net cloud mass flux profiles of convective parameterizations may, in practice, differ. First, vertical mass fluxes associated with stratiform rainfall will undermine the first-order balance between net cloud heating and clear sky radiative cooling. Second, the static stability in the lower troposphere of actively convecting regions differs from a moist adiabat by up to 30% [*Folkins and Martin*, 2005]. The radiative mass flux can be expressed as $\omega_r = Q_r/\sigma$, where Q_r is the radiative heating rate, and σ is the static stability. To the extent that a convective scheme drives the temperature profile toward a moist adiabat, it will introduce errors in σ and ω_r in the lower troposphere. Third, convective schemes tend to be poorly constrained by observed relative humidities above 10 km. Any deviation in upper tropospheric relative humidity from observations will introduce errors in ω_r. Finally, the clear sky radiative mass fluxes generated by convective schemes can be very sensitive to small errors in temperature, especially in the upper troposphere of actively convecting regions, where the moist adiabat approaches a dry adiabat and the static stability is very small.

[19] Figure 4 shows the tropical mean net cloud mass fluxes of the four models. The "top heavy" divergence profiles of the TCM and CONRAD (Emanuel) models are associated with net cloud mass flux profiles which peak in the upper troposphere. Figure 4 also shows the net cloud mass fluxes generated by two versions of a free running general circulation model. The solid black line shows the net cloud mass flux of the standard version of the atmospheric component AM2 of the Geophysical Fluid Dynamics Laboratory (GFDL) coupled climate model CM2 [*Delworth et al.*, 2006]. It uses the RAS convective parameterization. The dashed line shows the net cloud flux of an alternate version of this model which uses the Donner parameterization [*Donner et al.*, 2001; L. J. Donner et al.,

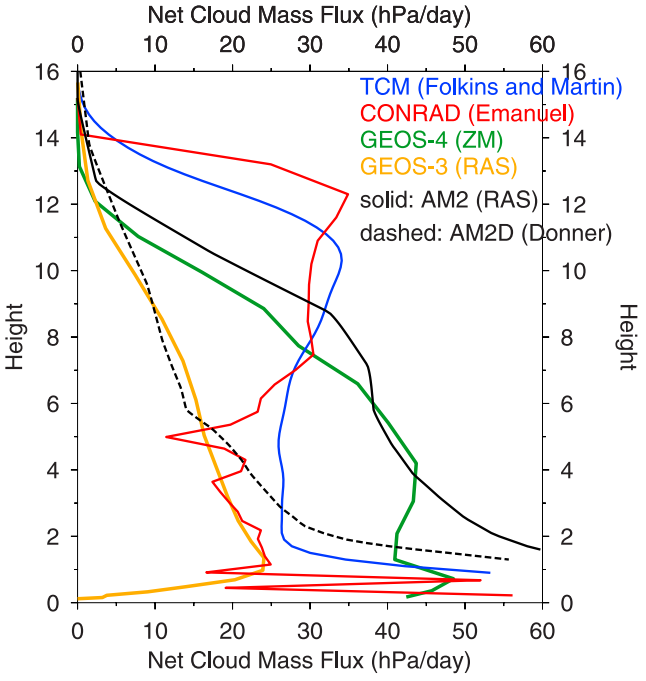

Figure 4. Net cloud (updraft plus downdraft) mass fluxes of the four models used in this study (colored lines) and net cloud mass flux of the standard version of the AM2 model (solid black lines). The dashed black line shows a version of the AM2 model using the Donner parameterization.

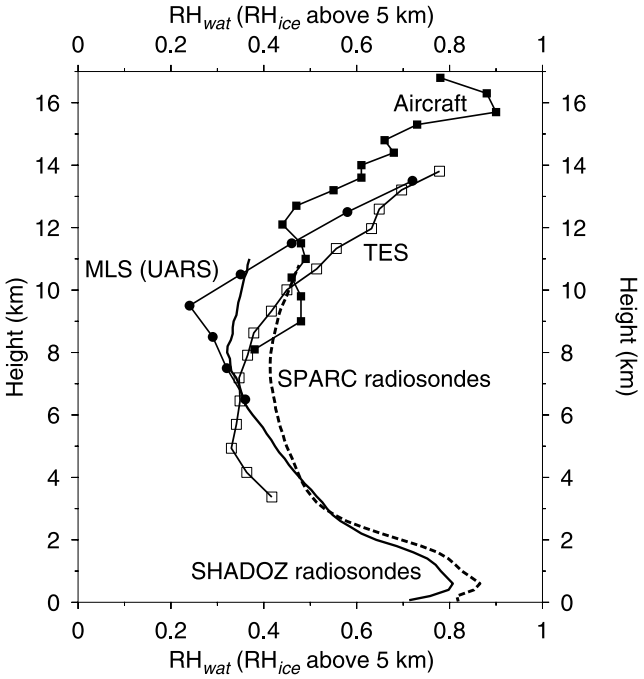

Figure 5. A compilation of various tropical mean (20°S–20°N) relative humidity climatologies demonstrating the overall C-shaped profile in the tropics: SHADOZ radiosondes (solid lines), SPARC radiosondes (dashed line), Tropospheric Emission Spectrometer (TES) (solid line with boxes), Microwave Limb Sounder (MLS) from the Upper Atmosphere Research Satellite (UARS) (solid line with bullets), and an aircraft climatology (solid line with solid boxes). Measurements from TES were excluded if the relative humidity with respect to ice exceeded 150%.

Transport of radon-222 and methyl iodide by deep convection in the GFDL global atmospheric model AM2, submitted to *Journal of Geophysical Research*, 2006, hereinafter referred to as Donner et al., submitted manuscript 2006], and is labeled AM2D. The weaker net cloud mass flux of the AM2D model as compared with AM2 is at least partially attributable to the stronger stratiform rainfall component in this version of the model. The AM2 (RAS) and GEOS-4 (ZM) net cloud mass fluxes are similar to each other, as are the AM2D (Donner) and GEOS-3 (RAS) net cloud mass fluxes. This suggests that there is a wide range of net convective mass flux profiles in both free running general circulation and forecast models [see also *Mahowald et al.*, 1995], and that changes in the implementation of a convective scheme (here RAS) can have a dramatic impact on the net cloud mass flux generated by the scheme.

6. Water Vapor

[20] Tropical water vapor mixing ratios decrease by roughly four orders of magnitude in going from the surface to the cold point tropopause. This variation contributes to the difficulty of measuring water vapor mixing ratios with a single instrument. Figure 5 shows a compilation of relative humidity measurements from several instruments.

[21] Two of the relative humidity profiles shown in Figure 5 are averages over radiosonde networks: the Stratospheric Processes and their Role in Climate (SPARC) radiosonde network and the Southern Hemisphere Additional Ozonsesonde (SHADOZ) network [*Thompson et al.*, 2003]. These radiosonde networks were also used to calculate the tropical mean radiative mass fluxes of the TCM model. The average relative humidity of the SPARC stations is somewhat higher than the average relative humidity of the SHADOZ stations, presumably because most of the SPARC radiosonde locations between 20°S and 20°N are in the Western Tropical Pacific and Caribbean [*Folkins and Martin*, 2005]. Radiosondes typically have a dry bias in the upper troposphere [*Miloshevich et al.*, 2004]. Relative humidities from these two networks are therefore not shown above 11 km.

[22] The aircraft climatology [*Folkins et al.*, 2002b] was generated using water vapor measurements from three high-altitude aircraft campaigns: the 1987 Stratospheric Tropospheric Exchange Project (STEP) [*Kelly et al.*, 1993], the 1993 Central Equatorial Pacific Experiment (CEPEX) [*Weinstock et al.*, 1995], and the 1994 Airborne Southern Hemisphere Ozone Experiment/Measurements for Assessing the Effects of Stratospheric Aircraft) (ASHOE/MAESA) campaign. Most of the flights from these three campaigns occurred in the Western Tropical Pacific. The aircraft climatology may therefore be biased toward high relative humidity. However, this is probably less of a concern in the upper troposphere, where the stronger horizontal winds tend to increase the spatial scale of relative humidity anomalies [*Salby et al.*, 2003].

[23] The aircraft climatology is reasonably consistent with the relative humidity climatology from the Microwave Limb Sounder (MLS) instrument [*Read et al.*, 2001], part of the Upper Atmosphere Research Satellite (UARS).

[24] The aircraft climatology is also in reasonable agreement with a tropical mean relative humidity climatology from the Tropospheric Emission Spectrometer (TES), an instrument on the Aura Spacecraft. TES has been measuring water vapor mixing ratios and temperatures since its launch in July 2004 [*Beer*, 2006]. The TES retrievals are based on the optimal estimation method [*Rodgers*, 2000], and are described more fully by *Worden et al.* [2004], *Bowman et al.* [2006], and *Kulawik et al.* [2006]. TES measurements generally agree with coincident measurements from the Atmospheric Infrared Sounder (AIRS) to 1 K in temperature, and ±20% in water vapor mixing ratio. The vertical resolution of the TES and MLS instruments is inherently more coarse than the sondes, and is on the order of 2 to 4 km. The TES relative humidity climatology shown in Figure 5 was obtained from 5500 version FO3_O2 profiles, and spans the period 21 May 2005 to 2 March 2006, with more frequent observations during January and February of 2006. Although no cloud screening was applied, profiles in which the radiance rms residual exceeded 1.4 were removed.

[25] Figure 6 shows tropical mean water vapor mixing ratios from the TES and MLS (UARS) instruments, the aircraft climatology, the Halogen Occultation Experiment (HALOE) [*Grooss and Russell*, 2005], and from the Atmospheric Chemistry Experiment Fourier Transform Spectrometer (ACE-FTS) [*Bernath et al.*, 2005; *Boone et al.*, 2005].

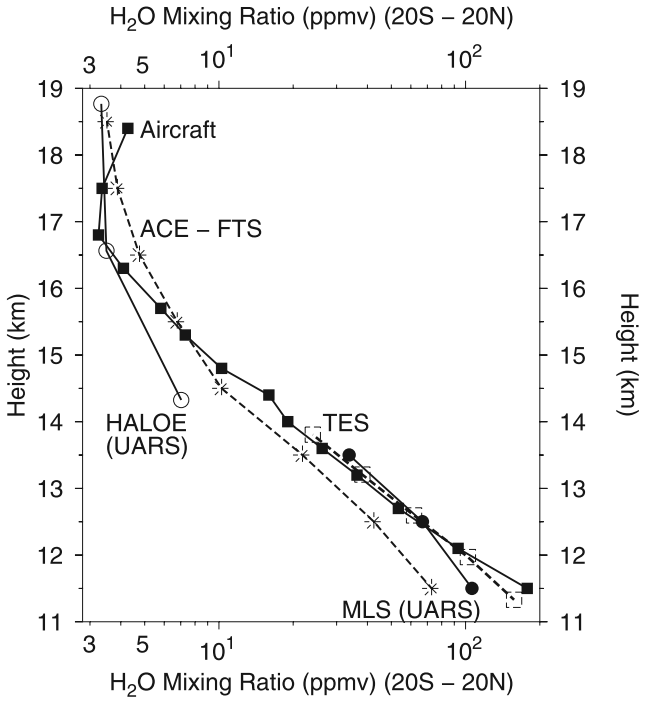

Figure 6. A compilation of various tropical mean (20°S–20°N) water vapor mixing ratio climatologies: ACE FTS (dashed line with asterisks), Halogen Occultation Experiment (solid line with open circles), Microwave Limb Sounder (solid line with bullets), Tropospheric Emission Spectrometer (TES) (dashed line with open boxes), and an aircraft climatology (solid line with solid boxes).

[26] ACE-FTS measured approximately 270 profiles of water vapor in the tropics (20°S–20°N) between 1 February 2004 and November 2005. It determines the mixing ratios of a diverse suite of chemical species through a vertical scan of the absorption of infrared solar radiation by the atmosphere during sunrise and sunset viewing geometries. In principle, it can obtain profiles extending to the surface. However, cloud effects substantially reduce the frequency of measurements in the troposphere. ACE-FTS has a vertical resolution of 4 km. The profiles used here are reported on a 1 km grid.

[27] Above 16 km, the HALOE, ACE-FTS, and aircraft water vapor mixing ratio climatologies shown in Figure 6 are in reasonably good mutual agreement. The HALOE water vapor mixing ratios are somewhat lower than the other climatologies below 15 km.

[28] Figure 7 compares the aircraft and SHADOZ relative humidity climatologies with those from the GEOS-3, GEOS-4, and CONRAD (Emanuel) models. The relative humidity of the TCM model is not shown because it inputs observed relative humidities as a constraint. The GEOS-3 relative humidity is in good agreement with the observational climatologies below 13 km. The increase in GEOS-4 relative humidity near 7 km is associated with an increase in convective detrainment near the same altitude (Figure 3). The onset of this increase is several km lower than in most of the relative humidity climatologies shown in Figure 5.

[29] The increase in observed relative humidity above 10 km has been attributed to an increase in convective detrainment near the same altitude [*Folkins et al.*, 2002b]. The relative humidity of the CONRAD (Emanuel) model also starts increasing near 10 km, with a sharp peak near 14 km, apparently caused by the sharp peak in convective detrainment at the same altitude. The weak upper tropospheric detrainment rates of the GEOS-3 and GEOS-4 models may explain the dry bias of these models above 13 km.

[30] Figure 7 also shows that the relative humidity of the CONRAD (Emanuel) is larger than the SHADOZ climatology in the lower troposphere. The CONRAD (Emanuel) model is tuned, in part, to be consistent with radiosonde humidity measurements from the TOGA/COARE experiment [*Emanuel and Zivkovic-Rothman*, 1999]. This experiment occurred in a region north of Australia characterized by frequent deep convection and enhanced lower-tropospheric relative humidities. It is likely that the CONRAD (Emanuel) scheme would generate a tropical mean relative humidity in better agreement with observations when implemented in a three-dimensional model. In a one-dimensional framework, where it is assumed that mixing between cloudy outflow and the background atmosphere is effectively instantaneous, there is a tendency to overestimate the mean relative humidity [e.g., *Nilsson and Emanuel*, 1999]. In practice, the horizontal transport of lower-tropospheric moisture from regions with frequent deep convective to regions of preferred subsidence is too slow to prevent the development of reduced relative humidities in subsidence regions. Nonlinear effects associated with these regional

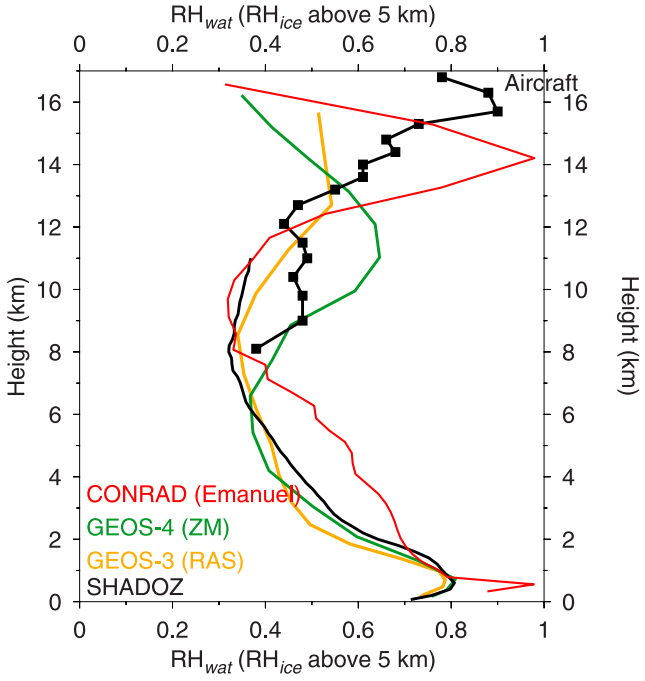

Figure 7. A comparison of the aircraft (black line with solid boxes) and SHADOZ radiosonde (solid black line) relative humidity climatologies in the tropics (20°S–20°N) with four model simulations. The relative humidity profiles of the GEOS-3 and GEOS-4 models are for 1 July 2001.

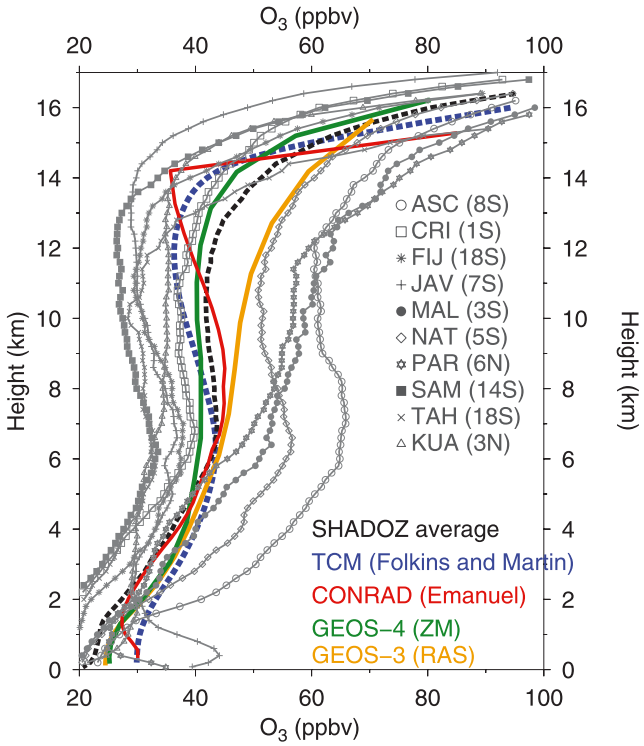

Figure 8. Ozone climatologies from locations between 20°S and 20°N that are part of the Southern Hemisphere Additional Ozonsesonde (SHADOZ) network (grey curves) and an average over the 10 SHADOZ locations shown (thick dashed black line). The four colored ozone profiles correspond to the models indicated. The SHADOZ locations are ASC, Ascension Island; CRI, San Cristobal; FIJ, Fiji; JAV, Watukosek, Java; MAL, Malindi; NAT, Natal; PAR, Paramaribo; SAM, American Samoa; TAH, Tahiti; and KUA, Kuala Lumpur.

inhomogeneities may undermine the accuracy of a one-dimensional tropical mean approach.

7. Calculation of Trace Species Profiles

[31] The GEOS-Chem model was used to generate tropical mean annual profiles of O_3, CO, and HNO_3 from the 2001 GEOS-3 and GEOS-4 winds, temperatures, and convective mass fluxes. GEOS-Chem is an off-line Chemical Transport Model (CTM) which can be run using various assimilated meteorological data sets [*Bey et al.*, 2001]. Version V7-01-02 of GEOS-Chem http://www-as.harvard.edu/chemistry/trop/geos) is used here.

[32] In a three-dimensional model, the simulation of tracer mixing ratios in the upper tropical troposphere will be sensitive to the way these tracers are modeled in the stratosphere. In GEOS-Chem, ozone in the stratosphere is calculated using a method [*McLinden et al.*, 2000] in which ozone is released into the lower tropical stratosphere (between 30°S and 30°N and 70 to 10 hPa) at a prescribed rate and subsequently passively advected [*Bey et al.*, 2001].

[33] Lightning is the main source of NO_x to the upper tropical troposphere, and therefore plays an important role in the budgets of O_3 and HNO_3. In GEOS-Chem, the emission of lightning NO_x is linked to deep convection using a parameterization [*Price and Rind*, 1992] and vertical profile [*Pickering et al.*, 1998] implemented by *Wang et al.* [1998]. The global emission of lightning was fixed at 5 Tg N/year.

[34] To generate species profiles using the CONRAD (Emanuel) model, mixing ratios of O_3 and CO were fixed in the boundary layer. The model then calculates a tracer concentration within updrafts and downdrafts, as well as the background atmosphere. At each model level, tracers are affected by both entrainment and detrainment mass fluxes. However, chemical tendencies are applied to the tracer only in the background atmosphere.

[35] The TCM model generates a vertical profile of the mixing ratio of a tracer $[X]$ using the expression

$$\frac{\partial [X]}{\partial t} = -(\omega r + \omega e)\frac{\partial [X]}{\partial p} + P - L[X] + d\left([X]_{\mathrm{conv}} - [X]\right). \quad (1)$$

[36] ω_r and ω_e are the evaporative and radiative mass fluxes in the clear sky column (expressed as pressure velocities). P is the rate of production of the tracer (e.g., in ppbv/day), and L is the loss rate (day^{-1}). The detrainment rate d is the rate at which the cloudy column injects air into the clear sky column, and is related to the clear sky column mass fluxes through

$$d = \frac{\partial(\omega_r + \omega_e)}{\partial p}. \quad (2)$$

[37] The first term on the right hand side of (1) represents vertical advection of $[X]$ by radiative subsidence and clear sky downdrafts. The second and third terms on the right represent in situ chemical production and loss, while the fourth term represents the effect of cloudy outflow. The parameter $[X]_{\mathrm{conv}}$ in (1) refers to the mean mixing ratio of the tracer in air detraining from convective clouds. For a given chemical species, it is the only free parameter of the model. The radiative and downdraft mass fluxes are diagnosed from tropical mean temperatures and humidities, while the rates of chemical production and loss can be independently specified by observations, or some other model. In this paper, we assume that the tropical mean profile of the tracer is independent of time.

[38] Differences in trace gas profiles between the four models can arise from either transport or chemistry. To minimize differences arising from chemistry, tropical mean estimates for the rates of chemical production and loss in the TCM and CONRAD (Emanuel) models were obtained, where possible, from the GEOS-Chem chemical mechanism using GEOS-4 meteorology.

8. Ozone

[39] Ozonesondes have been launched since 1998, typically biweekly, at various tropical locations as part of the SHADOZ campaign [*Thompson et al.*, 2003]. Figure 8 shows annual mean ozone profiles at eleven SHADOZ stations between 20°S and 20°N. The profiles fall into two discrete groups. Ozone mixing ratios at locations near Africa or South America, such as Natal (Brazil), Paramaribo

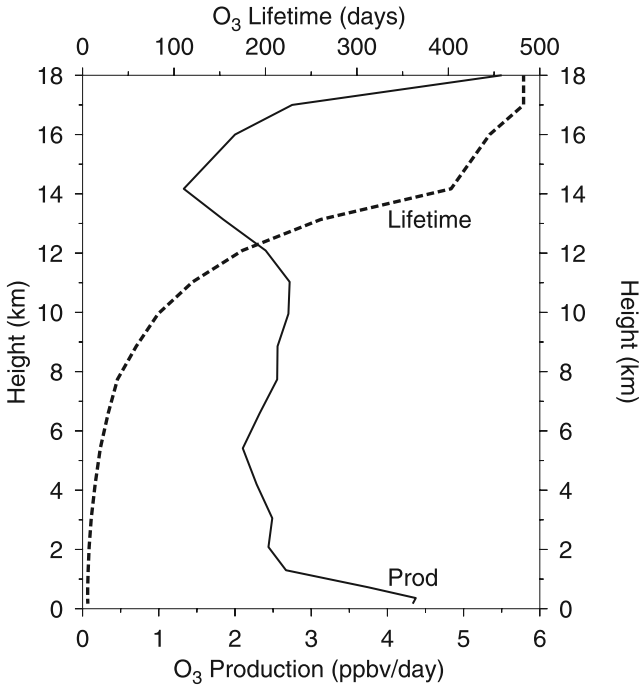

Figure 9. Rate of production of ozone, and its lifetime against photochemical loss, used to calculate the mean ozone profiles of the CONRAD (Emanuel) and TCM (Folkins and Martin) models. Below 14 km, the profiles were generated using the GEOS-Chem off-line chemical transport model using GEOS-4 meteorology. Above 14 km, they were calculated from ASHOE/MAESA and STRAT measurements using a procedure discussed in the text.

(Surinam), Ascension (Atlantic Ocean), and Malindi (Kenya), are significantly larger than locations more strongly influenced by marine convection, such as Java, Samoa, Fiji, San Cristobal (Galapagos), Tahiti, and Kuala Lumpur. This wave-1 pattern in tropical ozone has been attributed largely to the upper tropospheric ozone production from lightning generated NO_x, coupled with persistent subsidence over the tropical Atlantic region [*Martin et al.*, 2002].

[40] Tropical mean estimates for the photochemical production P of ozone, and its lifetime against photochemical loss (i.e., 1/L), are shown in Figure 9. Below 14 km, these estimates were taken from the GEOS-Chem model using GEOS-4 meteorology. Above 15 km, it was assumed that ozone was produced exclusively by the $NO + HO_2$ reaction and O_2 photolysis, and that ozone was destroyed by reaction with HO_2 and OH. The rates of these reactions were determined from aircraft measurements from ASHOE/MAESA, and the 1995–1996 Stratospheric Tracers of Atmospheric Transport (STRAT) experiment.

[41] The six marine profiles in Figure 8 have an ozone minimum near 12 km. In the TCM model, this minimum is associated with a maximum in deep convective outflow at the same altitude. Deep convection is effective at maintaining ozone mixing ratios significantly below the values predicted by the assumption local photochemical steady state. For example, using $[O_3]_{conv}$ = 30 ppbv in the TCM model generates an ozone mixing ratio at 12 km of 36 ppbv, whereas the ozone lifetime and production rates shown in Figure 9 generate a steady state ozone mixing ratio at 12 km of 420 ppbv. The rapid increase in ozone mixing ratios above 13 km is mainly due to a decrease in convective outflow. The weakening of this dynamical forcing allows ozone mixing ratios to more closely approach photochemical steady state.

[42] The TCM model (dashed blue curve) simulates the shape of tropical mean ozone profiles reasonably well, especially in marine regions. It does, however, underestimate the SHADOZ tropical mean profile (dashed black curve). This may be partly because marine locations are somewhat underrepresented in the SHADOZ average relative to their area. It may also be due to the absence in the TCM model of quasi-horizontal transport of stratospheric ozone into the upper tropical troposphere across the subtropical jets. Although there is significant evidence that this pathway is a source of ozone to the upper tropical troposphere [e.g., *Folkins et al.*, 1999; *Zachariasse et al.*, 2001; *Marcy et al.*, 2004], its magnitude is not well quantified.

[43] The mean ozone profile of the GEOS-4 model (green curve) is in excellent agreement with the SHADOZ mean ozone profile. The GEOS-3 model (orange curve) overestimates ozone in the upper troposphere, presumably because its convective forcing in this region is too weak.

[44] The ozone profile of the CONRAD (Emanuel) model was generated by setting the ozone mixing ratio in the boundary layer equal to 30 ppbv. This profile, shown in red, has a pronounced upper tropospheric ozone minimum. The altitude of this minimum is somewhat higher and more pronounced than in the SHADOZ climatology. This is consistent with previous work suggesting that the implementation of this convective parameterization in a three-dimensional model gives rise to excessive convective outflow close to the tropical tropopause [*Peng et al.*, 2004]. Above 14 km, the ozone mixing ratios of the CONRAD (Emanuel) model are likely to be sensitive to the value of the imposed large-scale velocity.

[45] The lifetime of ozone with respect to photochemical destruction is extremely short in the tropical marine boundary layer. Ozone mixing ratios in the tropical marine boundary layer are therefore typically very low, usually less than 20 ppbv. This ozone depleted air is injected into the upper troposphere by deep convection, giving rise to the upper tropospheric minimum shown in Figure 8. The net rate of in situ ozone production is usually positive above 5 km, so that above this altitude, the fraction of air parcels whose ozone mixing ratio is less than 20 ppbv is a useful proxy for the rate of deep convective outflow [*Folkins et al.*, 2002a; *Solomon et al.*, 2005]. Figure 10 shows a vertical profile of the fraction of ozone measurements less than 20 ppbv above Samoa. As would be expected, the incidence of low ozone mixing ratios exhibits an upper tropospheric maximum coincident with a peak in convective detrainment, as calculated from the TCM model. This fraction decreases toward the tropical tropopause as the frequency of quasi undilute convective outflow diminishes. The low ozone fraction also exhibits a midtropospheric minimum, consistent with reduced convective outflow. The increase in the low ozone fraction below 6 km may be associated with a simultaneous increase in the rate of shallow convective outflow, as occurs in the TCM model.

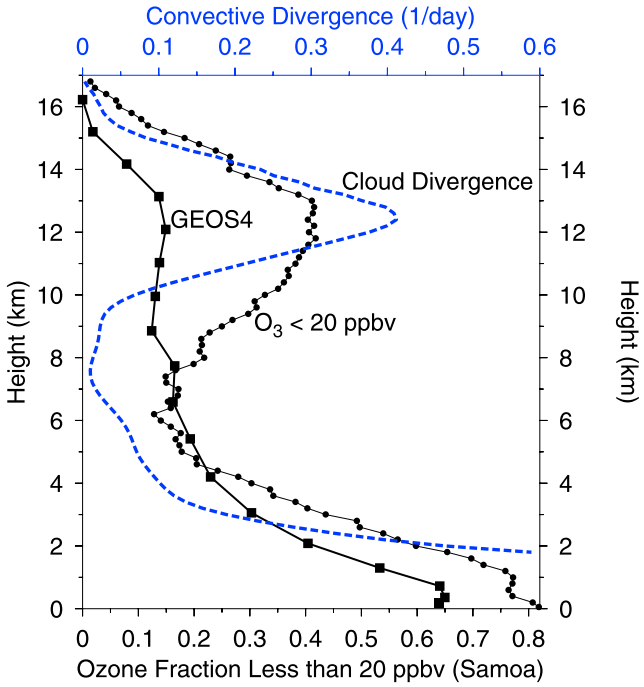

Figure 10. Cloud detrainment profile of the two-column model (TCM) (dashed line) (also shown in Figure 3); fraction of air parcels (curve with small circles), as a function of altitude, whose ozone mixing ratio is less than 20 ppbv, calculated using the SHADOZ ozonesondes launched from Samoa; and ozone fraction (curve with solid boxes), also from Samoa, as calculated from the 2001 GEOS-4 simulation, archived at hourly resolution.

[46] Figure 10 also shows the fraction of ozone measurements less than 20 ppbv as a function of altitude above Samoa using 12 months of hourly data from the GEOS-4 simulations. This modeled fraction has less variation with altitude than the observations, presumably reflecting the tendency, in the GEOS-4 implementation of the ZM convective parameterization, to detrain air over a broad range of altitudes.

9. Carbon Monoxide

[47] In the tropics, large amounts of carbon monoxide are generated at the surface by biomass burning. The dominant in situ sources of CO are the oxidation of methane and shorter-lived hydrocarbons, with methane oxidation becoming the main source in aged air masses and the lower stratosphere. The only significant chemical sink of CO in the troposphere is OH attack. Estimates for the rate of CO production by in situ chemistry, as well as its lifetime against OH attack, are shown in Figure 11. Below 14 km, these profiles were again obtained by averaging over the rates of production and loss calculated by the GEOS-Chem model using GEOS-4 meteorology. Above 15 km, it was assumed that the only source of CO is methane oxidation. The rates of photochemical production and loss were then determined from OH measurements taken during ASHOE/MAESA and STRAT.

[48] Figure 12 is a compilation of tropical CO measurements from the ACE-FTS instrument, and from various aircraft campaigns. Below 14 km, one would expect a tropical mean climatology of CO to be relatively featureless, since the photochemical lifetime of CO (~40 days) is much longer than the timescale for convective replacement. Though true for the most part, CO enhancements from Asian outflow during PEM West B [*Talbot et al.*, 1997], and from African biomass burning during the Transport and Atmospheric Chemistry in the Atlantic (TRACE-A) experiments [*Chatfield et al.*, 1998], give rise to regional enhancements in CO which affect the overall GTE average.

[49] Because of its long photochemical lifetime, CO is most useful as a chemical tracer for diagnosing the shape of the high-altitude tail of the deep convective divergence profile [*Dessler*, 2002]. In this region, CO assumes a mixing ratio which is intermediate between its photochemical steady state value and its mean convective detrainment value. Figure 13 is a comparison of the ACE-FTS CO climatology with profiles generated by the four model simulations. CO mixing ratios from the GEOS-4 simulation start decreasing near 11 km. This appears to be associated with an onset of a decrease in convective outflow near the same altitude. By 14 km, the GEOS-4 model significantly underestimates the mean ACE-FTS CO mixing ratio. Both GEOS-3 and GEOS-4 lack the sharp decrease in ACE-FTS CO mixing ratios that occurs above 14 km. Above 16 km, the GEOS-3 and GEOS-4 models tend to overestimate CO. Given the relatively weak convective outflow in these models above 14 km, this overestimate may indicate exces-

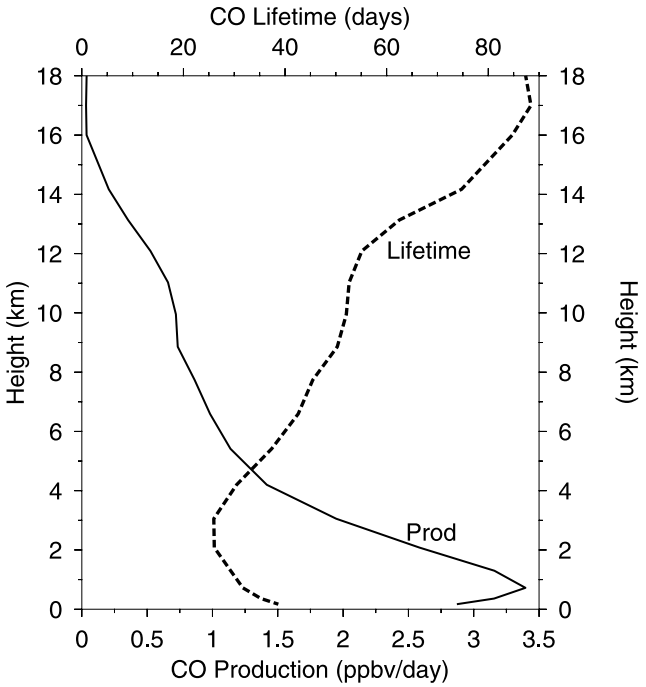

Figure 11. An estimate of the tropical mean production of carbon monoxide, and its lifetime against photochemical loss. These estimates were used in the CONRAD (Emanuel) and TCM (Folkins and Martin) models to calculate the CO profiles shown in Figure 9. Their derivation is described in the text.

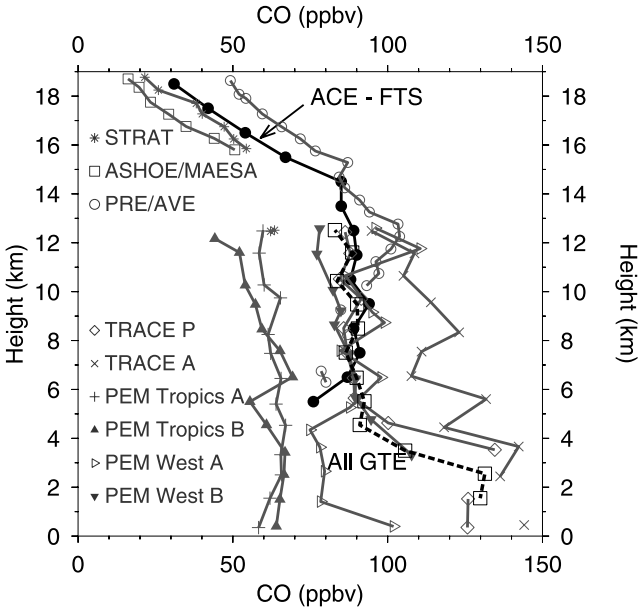

Figure 12. Tropical (20°S–20°N) CO climatologies from the ACE-FTS instrument and from various aircraft campaigns. The thick dashed line is an average over all four Pacific Exploratory Experiment (PEM) campaigns and the two Transport and Atmospheric Chemistry (TRACE) campaigns.

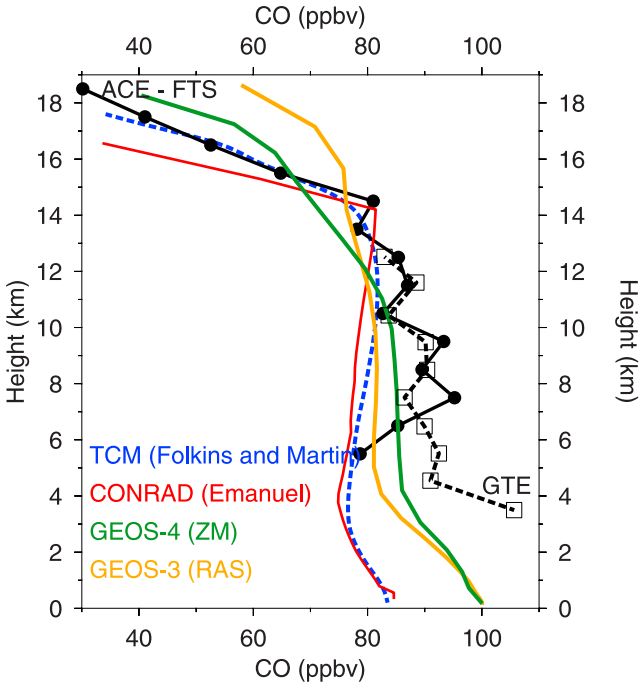

Figure 13. Model predictions of the tropical mean CO profile (four colored curves). They are compared with a climatology from ACE-FTS (solid curve with bullets) and an average over the seven GTE campaigns shown in Figure 12 (dashed curve with open boxes).

sive numerical diffusion of CO rich air from below. Above 15 km, OH mixing ratios in GEOS-Chem are prescribed [*Schneider et al.*, 2000] rather than internally calculated.

[50] The CO profile simulated by the TCM model is constrained to agree with the ACE-FTS model at 14 km by setting $[CO]_{conv}$ = 85 ppbv. The shape of the modeled CO profile is in good overall agreement with the ACE-FTS climatology, and in particular, with the observed CO gradient above 14 km. This agreement suggests that the shape of the convective outflow profile above 14 km in the TCM model is realistic.

[51] The boundary layer CO mixing ratio in the CONRAD (Emanuel) model was also set equal to 85 ppbv. The strong convective detrainment feature near 14 km gives rise to an upper tropospheric CO maximum near the same altitude. Above this altitude, CO mixing ratios decrease rapidly with altitude. As with ozone, the rate of this decrease would be sensitive to the value of the imposed large scale velocity.

10. Nitric Acid

[52] Figure 14 shows a tropical mean profile of HNO_3 measured by the ACE-FTS instrument (using a research version of retrieval version 2.2). HNO_3 has also been measured in the tropics by instruments on the NASA DC-8 during five aircraft campaigns conducted as part of the Global Tropospheric Experiment (GTE) [*Talbot et al.*, 1996, 1997]. Figure 14 shows tropical mean profiles of HNO_3 from each of these campaigns, as well as an overall GTE average. Most of the flights during the Pacific Exploratory Mission (PEM) West B campaign were designed to sample Asian outflow. This appears to have contributed to the large

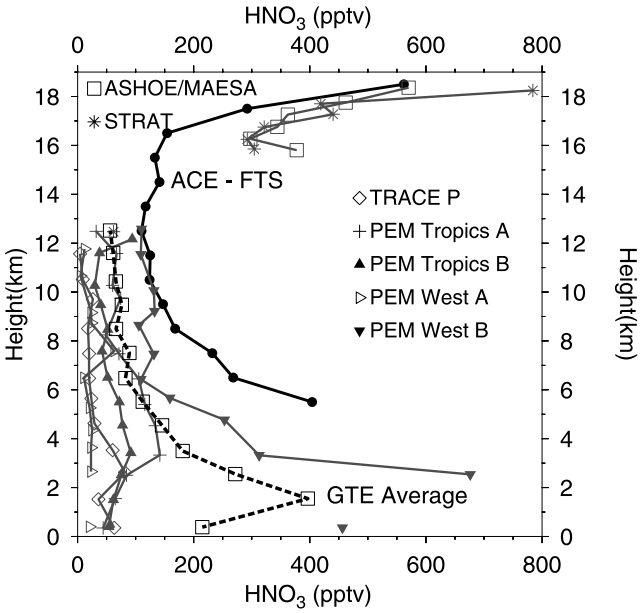

Figure 14. An intercomparison of tropical (20°S–20°N) HNO_3 climatologies from ACE-FTS and various aircraft campaigns. The thick dashed line is an average of the HNO_3 climatologies from the four Pacific Exploratory Mission (PEM) experiments and the Transport and Atmospheric Chemistry in the Pacific (TRACE-P) experiment. The ASHOE/MAESA and STRAT plots refer to inferred rather than directly measured nitric acid (i.e., $HNO_3^* = NO_y - NO_x$).

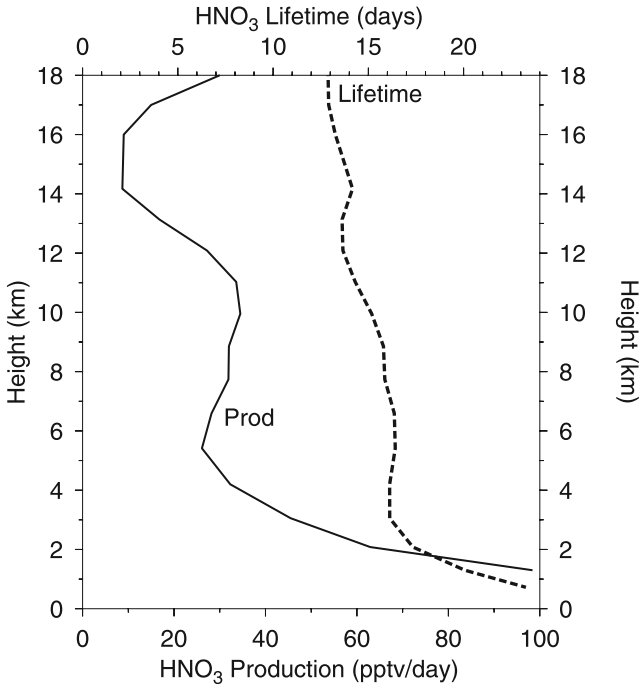

Figure 15. Rate of production of nitric acid (solid curve) and its lifetime against photochemical loss (dashed curve). These were used to calculate the mean nitric acid profiles of the CONRAD (Emanuel) and TCM (Folkins and Martin) models. Below 14 km, the profiles were generated using the GEOS-Chem off-line chemical transport model using GEOS-4 meteorology. Above 14 km, they were calculated from ASHOE/MAESA and STRAT measurements using a procedure discussed in the text.

increase in HNO_3 below 6 km in the average profile from this campaign. This large increase has a significant impact on the overall GTE average.

[53] HNO_3 was not directly measured from the ER-2 during the ASHOE/MAESA or STRAT experiments. HNO_3 should, however, be the dominant member of total reactive nitrogen (NO_y) above 16 km. In this case, $HNO_3^* = NO_y - NO_x$ should be a reasonably accurate upper limit for HNO_3. NO_x (= NO + NO_2) was inferred from the ER-2 measurements of NO and O_3 [*Fahey et al.*, 1996], and the standard photochemical steady state expression

$$[NO_2] = \frac{k_{NO+O_3}[O_3]}{J_{NO_2}}, \qquad (3)$$

where J_{NO_2} refers to the photolysis of NO_2. Figure 14 shows the mean profiles of HNO_3^* from the STRAT and ASHOE/MAESA ER-2 measurements. As would be expected, HNO_3^* is somewhat larger than HNO_3 from ACE-FTS, with at least some of the differences presumably attributable to additional NO_y species not measured from the ER-2, such as N_2O_5 and HO_2NO_2.

[54] The TCM model assumes that $[HNO_3]_{conv} = 0$, i.e., that the solubility of HNO_3 in water and ice is sufficiently high that HNO_3 is entirely removed during upward ascent within convective clouds. This appears to be a reasonable assumption, although the scavenging efficiency of nitric acid in cloud updrafts is probably not 100% [*Mari et al.*, 2000]. It is also assumes that evaporating precipitation is not a source of HNO_3 to the clear sky atmosphere.

[55] The main chemical source of HNO_3 is the NO_2 + OH reaction. The main chemical sinks of HNO_3 are photolysis and OH attack. Below 14 km, tropical mean expressions for these sources and sinks were obtained from the GEOS-Chem model using GEOS-4 meteorology. Above 14 km, they were determined from ASHOE/MAESA and STRAT measurements of OH [*Wennberg et al.*, 1998], NO_2 as inferred from O_3 and NO measurements described earlier, and the mean J_{HNO_3} photolysis rate along the tropical portions of the ASHOE/MAESA ER-2 flight tracks.

[56] Figure 15 shows the rate of production of HNO_3 in the TCM model, as well as the lifetime of HNO_3 against photochemical loss (1/L). The combined lifetime of HNO_3 against photolysis and OH attack is close to 15 days in most of the tropical troposphere. This lifetime is substantially longer than the convective replacement timescale of 2.5 days at the peak of the deep outflow mode in the TCM model. Convective outflow of air depleted in HNO_3 should therefore be the dominant negative forcing on upper tropospheric HNO_3 mixing ratios. Figure 16 shows that, in the TCM model, this convective forcing gives rise to a broad upper tropospheric minimum in HNO_3. The ACE-FTS profile also has a broad upper tropospheric HNO_3 minimum. However, this minimum is not as low as in the TCM model.

[57] The GEOS-3, GEOS-4, and TCM simulations of HNO_3 all compare reasonably well with the GTE and

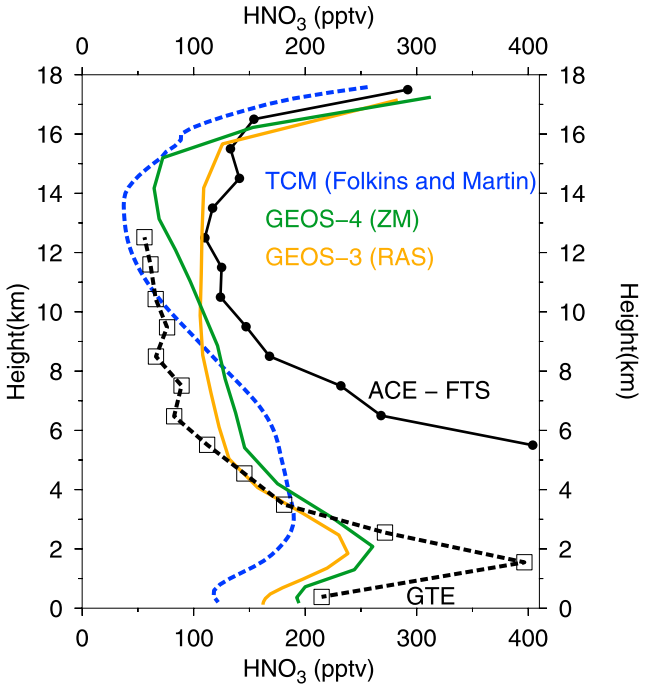

Figure 16. Nitric acid profiles generated by the GEOS-3, GEOS-4, and TCM models (colored curves). The solid black curve is a tropical (20°S–20°N) HNO_3 climatology obtained from ACE-FTS. The dashed curve is an average over the five Global Tropospheric Experiment (GTE) campaigns shown in Figure 15.

ACE-FTS averages shown in Figure 16. However, HNO_3 mixing ratios from ACE-FTS are larger than the GTE average at all altitudes where they overlap. Additional measurements of HNO_3 are needed to resolve this discrepancy and increase the usefulness of HNO_3 as a test of convective outflow in models.

[58] There is a rapid increase in ACE-FTS HNO_3 above 16 km. As convective outflow diminishes, one would expect a larger fraction of the ambient NO_y to originate from the stratosphere, i.e., from photochemical degradation of N_2O.

[59] In GEOS-Chem, the production of reactive nitrogen (NO_y) in the stratosphere, and the NO_x/HNO_3 ratio, were prescribed using monthly means from a two-dimensional model [*Schneider et al.*, 2000]. The imposition of this constraint probably contributes to the good agreement between the GEOS-3 and GEOS-4 models and ACE-FTS observations above 15.5 km.

11. Discussion and Conclusions

[60] There are multiple lines of evidence supporting the existence of a deep outflow mode in the tropics which starts near 10 km and has a maximum rate of convective outflow near 13 km: previous diagnostic studies [*Betts*, 1973; *Yanai et al.*, 1973; *Folkins and Martin*, 2005], tropical divergence profiles diagnosed from rawindsonde arrays [*Mapes and Houze*, 1993], the upper tropospheric ozone minimum, the high incidence of low ozone values in the upper tropical troposphere in regions characterized by active marine convection, the persistence of high tropical mean carbon monoxide mixing ratios to 14 km, and the onset of an increase in tropical mean relative humidity near 10 km. One objective of this paper has been to summarize previous chemical evidence in support of the deep outflow layer, and to integrate it with new evidence from ACE-FTS and other satellite instruments. Progress in the chemical characterization of the deep outflow layer has been slow, partly because its center of action lies within the data gap between the upper limit of the DC-8 GTE measurements ($\sim$12 km) and the typical lower limit of most ER-2 measurements ($\sim$15 km), and partly because of the reduced accuracy of radiosonde relative humidities above 11 km.

[61] The GEOS-3 implementation of the RAS convective parameterization does not exhibit a clearly defined deep outflow layer, and the rate of upper tropospheric convective detrainment in this model is quite weak. As a result, the ozone profile from GEOS-3 does not have an upper tropospheric ozone minimum, the onset of a decrease in carbon monoxide in the GEOS-3 model is lower than observed by ACE-FTS, and above 13 km, the GEOS-3 relative humidity is lower than the satellite and aircraft observations.

[62] It is difficult to come to general conclusions on the behavior of a convective scheme based on a particular implementation. The implementation of the RAS convective parameterization in the AM2 model is associated with a significantly larger net convective mass flux than in GEOS-3, and an upper tropospheric methyl iodide (CH_3I) maximum that would appear to be associated with a distinct deep outflow layer (Donner et al., submitted manuscript 2006). It is not clear whether these differences originate from differing amounts of stratiform rainfall in the two models, the role played by the assimilation of meteorological observations in the GEOS-3 model, or have some other explanation.

[63] The implementation of the ZM convective parameterization in the GEOS-4 model did generate a deep outflow layer. However, comparisons with ozone and relative humidity observations suggest that its onset is several km too low.

[64] The CONRAD (Emanuel) convective parameterization exhibits a very pronounced deep outflow layer. Ozone and relative humidity measurements suggest that this layer is somewhat high and overly sharply defined, at least in the one-dimensional implementation used here [see also *Peng et al.*, 2004].

[65] The generation of an appropriate separation between the shallow and deep outflow modes is likely to be a challenge for any bulk formulation of convective transport based on a single entraining plume. Approaches based on plume ensemble or stochastic mixing formulations allow for the possibility of relatively undilute outflow into the upper troposphere, and in principle, can more easily generate enhanced outflow in the upper tropical troposphere [see also *Lawrence and Rasch*, 2005].

[66] Because of reduced saturated water vapor pressures at very cold temperatures, the downdraft mass flux generated by a convective parameterization should be weak above 10 km. In the absence of a mass flux due to stratiform rainfall, the updraft mass flux should therefore be in approximate balance with the radiative mass flux. The radiative mass flux is mainly a function of the vertical profiles of temperature and relative humidity. Deep convective parameterizations which generate the correct upper tropospheric temperature and relative humidity profiles should also generate realistic deep outflow layers. Comparison with relative humidity measurements from satellite and aircraft, in concert with detailed comparisons with upper tropospheric temperature measurements, should therefore be regarded as an important test of a convective parameterization.

[67] The water vapor mixing ratios of air parcels detraining at the very cold temperatures of the deep outflow layer are very low. Subsidence of the extremely dry air is a strongly negative forcing on middle- and lower-tropospheric relative humidity. In order to generate relative humidities that are in agreement with observations, convective schemes with strongly enhanced outflow in the upper tropical troposphere are forced to evaporate large amounts of condensate in the middle and lower troposphere and therefore have much lower precipitation efficiencies than schemes which lack a pronounced deep outflow layer.

[68] Alternatively, it is difficult for a model with no downdraft parameterization (or evaporative moistening from stratiform rainfall) to generate a deep outflow layer. Such a model would be required to detrain saturated air at a broad range of altitudes in order to generate a relative humidity profile that is in reasonable agreement with observations. However, this approach would generate a mean relative humidity profile that agrees with observations using an incorrect physical mechanism.

[69] There are a number of important limitations to this study. It is not a direct intercomparison of convective

parameterizations. The convective mass fluxes and trace gas profiles generated by a parameterization will vary depending on whether it is implemented in a one-dimensional model, a three-dimensional assimilation model, or a free-running general circulation model. The most appropriate way to intercompare the tracer transport of various convectives scheme would be to run a single Chemistry Climate Model (CCM) with a variety of convective parameterizations, and with attention paid to any changes in vertical transport associated with stratiform rain. At this point, CCMs with full tropospheric chemistry are rare, so that intermediate comparisons using CTMs are useful. Running a convective parameterization in a one-dimensional framework is also useful because it gives insight into the intrinsic thermodynamic behavior of a convective scheme.

[70] The ACE-FTS measurements have provided the first observations of a broad upper tropospheric minimum in nitric acid. More generally, outflow in the deep outflow layer should be sufficiently rapid to diminish the concentration of any strongly water soluble species in this layer, provided the timescale with which in situ chemical production relaxes the species back to photochemical steady state is longer than a few days. The TCM model was able to reproduce the upper tropospheric minimum in HNO_3, as well as the overall shape of the HNO_3 profile, while making a number of simplifying assumptions: (1) that evaporating ice and water are not a significant source of HNO_3 to the clear sky atmosphere and (2) that absorption of clear sky HNO_3 onto falling ice or water does not contribute significantly to the vertical redistribution of HNO_3 in the tropics. The first assumption is consistent with the view that HNO_3 is efficiently removed from convective updrafts in the lower troposphere, so that only a small remnant fraction reaches the upper troposphere. Additional HNO_3 measurements are needed to make a more complete assessment of the role of gravitational settling of ice particles on the tropical HNO_3 budget [*Lawrence and Crutzen*, 1998].

[71] The rate of in situ chemical production of O_3 and HNO_3 is mainly determined by the ambient NO_x concentration. The main source of NO_x to the upper tropical troposphere is lightning. The injection of lightning generated NO_x into the upper tropical troposphere will be influenced by the vertical profile of convective outflow. In principle, studies using O_3 and HNO_3 as tracers of convective outflow should also include comparisons with NO_x observations, and use a lightning source profile that is interactively coupled with the convective parameterization.

[72] **Acknowledgments.** This research was supported by the Canadian Space Agency, the Canadian Foundation for Climate and Atmospheric Science, and the Natural Sciences and Engineering Council of Canada. We thank Kerry Emanuel for making the CONRAD model freely available and for helpful suggestions.

References

Beer, R. (2006), TES on the Aura mission: Scientific objectives, measurements and analysis overview, *IEEE Trans. Geosci. Remote. Sens.*, *44*, 1102–1105.

Bernath, P. F., et al. (2005), Atmospheric Chemistry Experiment (ACE): Mission overview, *Geophys. Res. Lett.*, *32*, L15S01, doi:10.1029/2005GL022386.

Betts, A. K. (1973), A composite mesoscale cumulonimbus budget, *J. Atmos. Sci.*, *30*, 597–610.

Bey, I., D. J. Jacob, R. M. Yantosca, J. A. Logan, B. Field, A. M. Fiore, Q. Li, H. Liu, L. J. Mickley, and M. Schultz (2001), Global modeling of tropospheric chemistry with assimilated meteorology: Model description and evaluation, *J. Geophys. Res.*, *106*, 23,073–23,096.

Bony, S., and K. A. Emanuel (2001), A parameterization of the cloudiness associated with cumulus convection: Evaluation using TOGA COARE data, *J. Atmos. Sci.*, *58*, 3158–3183.

Boone, C. D., R. Nassar, K. A. Walker, Y. Rochon, S. D. McLeod, C. P. Rinsland, and P. F. Bernath (2005), Retrievals for the atmospheric chemistry experiment Fourier-transform spectrometer, *Appl. Opt.*, *44*, 7218.

Bowman, K., et al. (2006), Tropospheric emission spectrometer: Retrieval method and error analysis, *IEEE Trans. Geosci. Remote Sens.*, *44*(5), 1297–1307.

Chatfield, R. B., et al. (1998), The great African plume from biomass burning: Generalizations from a three-dimensional study of TRACE-A carbon monoxide, *J. Geophys. Res.*, *103*, 28,059–28,077.

Delworth, T. D., et al. (2006), GFDL's CM2 global coupled climate models—Part I: Formulation and simulation characteristics, *J. Clim.*, *19*, 643–674.

Dessler, A. E. (2002), The effect of deep, tropical convection on the tropical tropopause layer, *J. Geophys. Res.*, *107*(D3), 4033, doi:10.1029/2001JD000511.

Donner, L. J., et al. (2001), A cumulus parameterization including mass fluxes, convective vertical velocities, and mesoscale effects: Thermodynamic and hydrological aspects in a general circulation model, *J. Clim.*, *14*, 3444–3463.

Emanuel, K. A. (1991), A scheme for representing cumulus convection in large-scale models, *J. Atmos. Sci.*, *48*, 2313–2335.

Emanuel, K. A., and M. Zivkovic-Rothman (1999), Development and evaluation of a convection scheme for use in climate models, *J. Atmos. Sci.*, *56*, 1766–1782.

Fahey, D. W., et al. (1996), In situ observations of NO_y, O_3, and the NO_y/O_3 ratio in the lower stratosphere, *Geophys. Res. Lett.*, *23*, 1653–1656.

Folkins, I., and R. V. Martin (2005), The vertical structure of tropical convection, and its impact on the budgets of water vapor and ozone, *J. Atmos. Sci.*, *62*, 1560–1573.

Folkins, I., M. Loewenstein, J. Podolske, S. Oltmans, and M. Proffitt (1999), A barrier to vertical mixing at 14 km in the tropics: Evidence from ozonesondes and aircraft measurements, *J. Geophys. Res.*, *104*, 22,095–22,102.

Folkins, I., C. Braun, A. M. Thompson, and J. C. Witte (2002a), Tropical ozone as an indicator of deep convection, *J. Geophys. Res.*, *107*(D13), 4184, doi:10.1029/2001JD001178.

Folkins, I., E. J. Hintsa, K. K. Kelly, and E. M. Weinstock (2002b), A simple explanation for the relative humidity increase between 11 and 15 km in the tropics, *J. Geophys. Res.*, *107*(D23), 4736, doi:10.1029/2002JD002185.

Folkins, I., P. Bernath, C. Boone, G. Lesins, N. Livesey, A. M. Thompson, K. Walker, and J. C. Witte (2006), Seasonal cycles of O_3, CO, and convective outflow at the tropical tropopause, *Geophys. Res. Lett.*, *33*, L16802, doi:10.1029/2006GL026602.

Grooss, J.-U., and J. M. Russell III (2005), Technical note: A stratospheric climatology for O_3, H_2O, CH_4, NO_x, HCl and HF derived from HALOE measurements, *Atmos. Chem. Phys.*, *5*, 2797–2807.

Hall, A., and S. Manabe (1999), The role of water vapor feedback in unperturbed climate variability and global warming, *J. Clim.*, *12*, 2327–2346.

Kelly, K. K., et al. (1993), Water vapor and cloud water measurements over Darwin during the STEP 1987 tropical mission, *J. Geophys. Res.*, *98*, 8713–8723.

Kulawik, S., et al. (2006), TES atmospheric profile retrieval characterization: An orbit of simulated observations, *IEEE Trans. Geosci. Remote Sens.*, *44*(5), 1324–1333.

Lawrence, M. G., and P. J. Crutzen (1998), The impact of cloud particle gravitational settling on soluble trace gas distributions, *Tellus, Ser. B*, *50*, 263–289.

Lawrence, M. G., and P. J. Rasch (2005), Tracer transport in deep convective updrafts: Plume ensemble versus bulk formulations, *J. Atmos. Sci.*, *62*, 2880–2894.

Mahowald, N. M., P. J. Rasch, and R. G. Prinn (1995), Cumulus parameterizations in chemical transport models, *J. Geophys. Res.*, *100*, 26,173–26,189.

Mapes, B., and R. A. Houze (1993), An integrated view of the 1987 Australian monsoon and its mesoscale convective systems: II: Vertical structure, *Q. J. R. Meteorol. Soc.*, *119*, 733–754.

Marcy, T. P., et al. (2004), Quantifying stratospheric ozone in the upper troposphere with in situ measurements of HCl, *Science*, *304*, 261–265.

Mari, C., D. J. Jacob, and P. Bechtold (2000), Transport and scavenging of soluble gases in a deep convective cloud, *J. Geophys. Res.*, *105*, 22,255–22,267.

Martin, R. V., et al. (2002), Interpretation of TOMS observations of tropical tropospheric ozone with a global model and in situ observations, *J. Geophys. Res.*, *107*(D18), 4351, doi:10.1029/2001JD001480.

McLinden, C., S. Olsen, B. Hannegan, O. Wild, M. Prather, and J. Sundet (2000), Stratospheric ozone in 3-D models: A simple chemistry and the cross-tropopause flux, *J. Geophys. Res.*, *105*, 14,653–14,665.

Miloshevich, L. M., A. Paukkunen, H. Vomel, and S. J. Oltmans (2004), Development and validation of a time-lag correction for Vaisala radiosonde humidity measurements, *J. Atmos. Oceanic Technol.*, *21*, 1305–1327.

Moorthi, S., and M. Suarez (1992), Relaxed Arakawa-Schubert: A parameterization of moist convection for general circulation models, *Mon. Weather Rev.*, *120*, 978–1002.

Nilsson, J., and K. A. Emanuel (1999), Equilibrium atmospheres of a two-column radiative-convective model, *Q. J. R. Meteorol. Soc.*, *125*, 2239–2264.

Peng, M. S., J. A. Ridout, and T. F. Hogan (2004), Recent modifications of the Emanuel convective scheme in the Navy operational global atmospheric prediction system, *Mon. Weather Rev.*, *132*, 1254–1269.

Pickering, K. E., Y. S. Wang, W. K. Tao, C. Price, and J. F. Muller (1998), Vertical distributions of lightning NO_x for use in regional and global chemical transport models, *J. Geophys. Res.*, *103*, 31,203–31,216.

Price, C., and D. Rind (1992), A simple lightning parameterization for calculating global lightning distributions, *J. Geophys. Res.*, *97*, 9919–9933.

Read, W. G., J. W. Waters, D. L. Wu, E. M. Stone, and Z. Shippony (2001), UARS Microwave Limb Sounder upper tropospheric humidity measurement: Method and validation, *J. Geophys. Res.*, *106*, 32,207–32,358.

Rodgers, C. D. (2000), *Inverse Methods for Atmospheric Sounding: Theory and Practice*, World Sci., Hackensack, N. J.

Salby, M., F. Sassi, P. Callaghan, W. Read, and H. Pumphrey (2003), Fluctuations of cloud, humidity, and thermal structure near the tropical tropopause, *J. Clim.*, *16*, 3428–3446.

Schneider, H. R., D. B. J. Jones, G.-Y. Shi, and M. B. McElroy (2000), Analysis of residual mean transport in the stratosphere: 1. Model description and comparison with satellite data, *J. Geophys. Res.*, *105*, 19,991–20,011.

Solomon, S., D. W. Thompson, R. W. Portmann, S. J. Oltmans, and A. M. Thompson (2005), On the distribution and variability of ozone in the tropical upper troposphere: Implications for tropical deep convection and chemical-dynamical coupling, *Geophys. Res. Lett.*, *32*, L23813, doi:10.1029/2005GL024323.

Stocker, T. F., et al. (2001), Physical climate processes and feedbacks, in *Climate Change 2001: The Scientific Basis,* chap. 7, pp. 418–470, Cambridge Univ. Press, New York.

Talbot, R. W., et al. (1996), Chemical characteristics of continental outflow from Asia to the troposphere over the western Pacific Ocean during September-October 1991: Results from PEM-West A, *J. Geophys. Res.*, *101*, 1713–1726.

Talbot, R. W., et al. (1997), Large-scale distributions of tropospheric nitric, formic, and acetic acids over the western Pacific basin during wintertime, *J. Geophys. Res.*, *102*, 28,303–28,313.

Thompson, A. M., et al. (2003), Southern Hemisphere Additional Ozonesondes (SHADOZ) 1998–2000 tropical ozone climatology: 1. Comparison with Total Ozone Mapping Spectrometer (TOMS) and ground-based measurements, *J. Geophys. Res.*, *108*(D2), 8238, doi:10.1029/2001JD000967.

Wang, Y., D. J. Jacob, and J. A. Logan (1998), Global simulation of tropospheric O3-NOx-hydrocarbon chemistry: 1. Model formulation, *J. Geophys. Res.*, *103*, 10,713–10,726.

Weinstock, E. M., E. J. Hintsa, A. E. Dessler, and J. G. Anderson (1995), Measurements of water vapor in the tropical lower stratosphere during the CEPEX campaign: Results and interpretation, *Geophys. Res. Lett.*, *22*, 3231–3234.

Wennberg, P. O., et al. (1998), Hydrogen radicals, nitrogen radicals, and the production of O_3 in the upper troposphere, *Science*, *279*, 49–53.

Worden, J., et al. (2004), Predicted errors of tropospheric emission spectrometer nadir retrievals from spectral window selection, *J. Geophys. Res.*, *109*, D09308, doi:10.1029/2004JD004522.

Yanai, M., S. Esbensen, and J. Chu (1973), Determination of bulk properties of tropical cloud clusters from large-scale heat and moisture budgets, *J. Atmos. Sci.*, *30*, 611–627.

Yano, Y., et al. (2004), Estimations of mass fluxes for cumulus parameterizations from high-resolution spatial data, *J. Atmos Sci.*, *61*, 829–842.

Zachariasse, M., H. Smit, P. Van Velthoven, and H. Kelder (2001), Cross-tropopause and interhemispheric transports into the tropical free troposphere over the Indian Ocean, *J. Geophys. Res.*, *106*(D22), 28,441–28,452.

Zhang, G. J., and N. A. McFarlane (1995), Sensitivity of climate simulations to the parameterization of cumulus convection in the Canadian Climate Centre General Circulation Model, *Atmos. Ocean*, *33*, 407–446.

P. Bernath, C. Boone, and K. Walker, Department of Chemistry, University of Waterloo, Waterloo, ON, Canada N2L 3G1.

L. J. Donner, Geophysical Fluid Dynamics Laboratory, NOAA, Princeton University, Princeton, NJ 08540, USA.

A. Eldering, Jet Propulsion Laboratory, Pasadena, CA 91109, USA.

I. Folkins, G. Lesins, and R. V. Martin, Department of Physics and Atmospheric Science, Dalhousie University, Halifax, NS, Canada B3H 3J5. (ian.folkins@dal.ca)

B.-M. Sinnhuber, Institute of Environmental Physics, University of Bremen, D-28359 Bremen, Germany.